

Delay and Power Expressions for a CMOS Inverter Driving a Resistive-Capacitive Load

VICTOR ADLER AND EBY G. FRIEDMAN

Department of Electrical Engineering, University of Rochester, Rochester, NY 14627

adler@ee.rochester.edu, friedman@ee.rochester.edu

Received June 24, 1996; Accepted October 17, 1996

Abstract. A delay and power model of a CMOS inverter driving a resistive-capacitive load is presented. The model is derived from Sakurai's alpha-power law and exhibits good accuracy. The model can be used to design and analyze those CMOS inverters that drive a large RC load when considering both speed and power. Expressions are provided for estimating the propagation delay and transition time which exhibit less than 27% discrepancy from SPICE for a wide variety of RC loads. Expressions are also provided for modeling the short-circuit power dissipation of a CMOS inverter driving a resistive-capacitive interconnect line which are accurate to within 15% of SPICE for most practical loads.

Key Words: interconnect, CMOS inverter model, interconnect delay, power dissipation, short-circuit power

I. Introduction

As the die size of CMOS integrated circuits continues to increase, interconnections have become increasingly significant [1]. With a linear increase in length, interconnect delay increases quadratically due to a linear increase in both interconnect resistance and capacitance [2]. Large interconnect loads not only affect performance but also cause excess power to be dissipated. A large RC load degrades the waveform shape, dissipating excessive short-circuit power in the following stages loading a CMOS logic gate.

Several methods have been introduced to reduce interconnect delay so that these impedances do not dominate the delay of a critical path [2–7]. Furthermore, with the introduction of portable computers, power has become an increasingly important factor in the circuit design process. Thus, power consumption must be accurately estimated when considering techniques for improving circuit speed when driving long interconnections. Therefore, circuit level models describing both dynamic power and, recently, short-circuit power have become increasingly important [8–11].

In this paper, an analytical expression for the transient response of a CMOS inverter driving a lumped RC load is presented. This approach is different from Kayssi *et al.* [12, 13] in that a lumped RC load is considered rather than a lossless capacitive load. Furthermore, Sakurai's alpha-power law [14] is used to describe the circuit operation of the CMOS transistors rather than the classical Shichman-Hodges model [15].

The alpha-power law model considers short channel behavior, permitting increased accuracy and generality in the delay and power expressions. These expressions are used to estimate the propagation delay and the rise and fall times (or transition times) of a CMOS inverter. Since the output waveform is accurately calculated, the short-circuit power [16] dissipated by the following stage can also be estimated. Furthermore, due to its relative simplicity, these expressions permit linear programming techniques to be used when optimizing the placement of buffers for both speed and power.

The paper is organized as follows: expressions for an inverter driving a lumped RC load are derived, and characteristic delay equations are presented and compared with SPICE in Section II. In Section III, expressions describing the dynamic, short-circuit, and resistive power dissipation of a CMOS inverter following a lumped RC load are introduced and compared with SPICE. Finally, some concluding remarks are offered in Section IV.

II. Transient Analysis of an RC Loaded CMOS Inverter

An analytical expression describing the behavior of an inverter driving a lumped RC load based on Sakurai's alpha-power law model [14] is presented. A diagram of this circuit is shown in Figure 1. In subsection A, the device model is described and an analytical expression

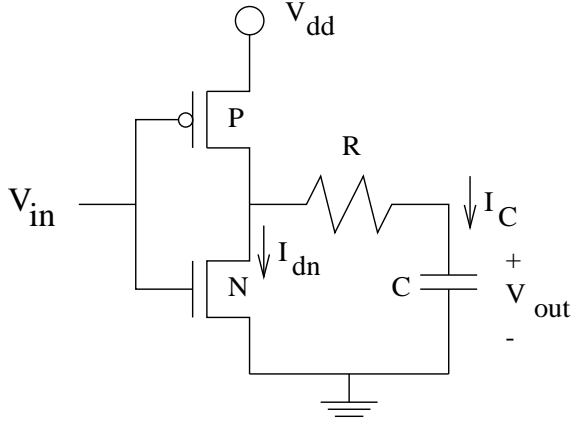


Fig. 1. A CMOS inverter driving an RC load.

for $V_{out}(t)$ is derived. In subsection B, several expressions that characterize the temporal properties of the circuit are presented. In subsection C, some results of the analytical expressions are presented along with comparisons to SPICE.

A. Derivation of Analytical Expressions

The alpha-power law model [14] accurately describes the effects of short channel behavior, such as velocity saturation, while providing a tractable equation. The linear region form of the alpha-power model is used to characterize the I-V behavior of the ON transistor since a large portion of the circuit operation occurs within this region under the assumption of a step or fast ramp input signal. When the input to the inverter is a unit step or fast ramp, V_{out} is initially larger than $V_{GS} - V_T$ for a shorter period of time than if the input to the inverter is a slow ramp. Therefore, the circuit operates in the linear region for a greater portion of the total transition time for a large RC load, particularly for large load resistances. When the load resistance is large, a large IR voltage drop occurs across the load resistor once the capacitor begins to discharge, thus V_{DS} is nearly immediately less than $V_{GS} - V_T$, as shown in Figure 2. The N-channel device operates in the linear region once the step input goes high when driving large RC loads. Note however if the input waveform increases more slowly or the load impedance is small, the inverter operates in the saturation region for a longer time before switching into the linear region.

Only the falling output (rising input) waveform is considered in this paper. The following analysis, how-

ever, is equally applicable to a rising output (falling input) waveform. The lumped load is modeled as a resistor in series with a capacitor. The current through the output load capacitance is the same magnitude and opposite sign as the N-channel drain current (the P-channel current is ignored under the assumption of a step or fast ramp input). The capacitive current is

$$i_C = C \frac{dV_{out}}{dt} = -i_d, \quad (1)$$

where C is the output capacitance, V_{out} is the voltage across the capacitance C , i_C is the current discharged from the capacitor, and i_d is the drain current through the N-channel device.

The N-channel linear drain current is given by [14]

$$-C \frac{dV_{out}}{dt} = i_d = \frac{I_{do}}{V_{do}} \left(\frac{V_{GS} - V_T}{V_{DD} - V_T} \right)^\alpha V_{ds}, \quad (2)$$

for $V_{GS} \geq V_T$, $V_{GS} - V_T \geq V_{DS}$.

In the alpha-power law model, I_{do} represents the drive current of the MOS device and is proportional to W/L , V_{do} represents the drain-to-source voltage at which velocity saturation occurs with $V_{GS} = V_{DD}$ and is a process dependent constant, and α models the process dependent degree to which velocity saturation affects the drain-to-source current. α is within the range $1 \leq \alpha \leq 2$, where $\alpha = 1$ corresponds to a device operating strongly under velocity saturation, while $\alpha = 2$ represents a device with negligible velocity saturation. V_{DD} is the supply voltage, and V_T is the MOS threshold voltage (where V_{TN} (V_{TP}) is the N-channel (P-channel) threshold voltage). An empirical method to determine technology specific values for I_{do} and V_{do} is described in the appendix.

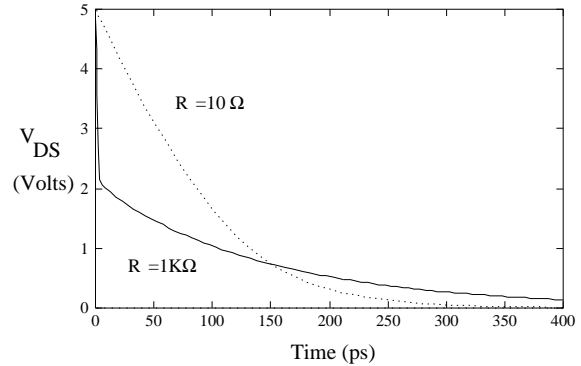


Fig. 2. Comparison of V_{DS} for a CMOS inverter driving different load resistances and a constant load capacitance ($C = 100$ fF).

Assuming a unit step input is applied to the circuit shown in Figure 1, V_{out} can be derived from (2). The linear equation, rewritten in Laplace form, is

$$\begin{aligned} SCV_{out} + S\mathcal{U}_{do}RCV_{out} + \mathcal{U}_{do}V_{out} \\ = CV_{out}(0) + \mathcal{U}_{do}RCV_{out}(0), \end{aligned} \quad (3)$$

where $\mathcal{U}_{do} = \frac{I_{do}}{V_{do}}$ is the saturation conductance.

Equation (3) yields

$$V_{out}(t) = V_{out}(0)e^{\frac{-\mathcal{U}_{do}}{\mathcal{U}_{do}RC+C}t}. \quad (4)$$

Graphs of $V_{out}(t)$ for a wide range of resistive and capacitive values (within practical limits) are shown in Figure 3. The analytical expression shown in (4) closely approximates SPICE for most of the region of operation for a wide range of load impedances from 10 Ω to 1000 Ω and from 10 fF to 1 pF. The maximum error of the output response derived from (4) as compared with SPICE (shown in Figure 3) is 25% for the specific case where the RC load is 10 Ω and 10 fF, approaching the unloaded case.

B. Analytical Delay Expressions

From (4), the propagation delay of a CMOS inverter calculated at the 50% point t_{PD} is

$$t_{PD} = .693 \frac{C + \mathcal{U}_{do}RC}{\mathcal{U}_{do}}. \quad (5)$$

The transition time of a CMOS inverter driving a lumped RC load calculated at the 90% point t_t is

$$t_t = 2.3 \frac{C + \mathcal{U}_{do}RC}{\mathcal{U}_{do}}. \quad (6)$$

Additional delay expressions that are used in section III B for determining the short-circuit power are

$$t_{V_{TN}} = \ln\left(\frac{V_{TN}}{V_{DD}}\right) \frac{C + \mathcal{U}_{do}RC}{\mathcal{U}_{do}} \quad (7)$$

and

$$t_{V_{TP}} = \ln\left(\frac{V_{DD} + V_{TP}}{V_{DD}}\right) \frac{C + \mathcal{U}_{do}RC}{\mathcal{U}_{do}}. \quad (8)$$

These equations describe the time for the output voltage to change by a threshold voltage from either ground or V_{DD} for an N-channel or P-channel device, respectively. Note that V_{TP} is negative.

C. Analysis of Delay Expressions

The accuracy of the analytic model as compared with SPICE is tabulated in Table I for a wide variety of output load resistances and capacitances. The interconnect resistance and capacitance are described in the first two columns of Table I, respectively. The transition times determined by the analytical expression and by SPICE are shown in the third and fourth columns, respectively. The propagation delay times determined by the analytical expression and by SPICE are listed in columns five and six, respectively. The error of the analytical expressions versus SPICE for the transition time and propagation delay is shown in the final two columns. A 0.8 μm CMOS technology is assumed. Note that the maximum error of the transition time t_t as compared with SPICE is 27%, and the maximum error of the propagation delay t_{PD} as compared with SPICE is 25%.

As noted above, (5) and (6) can be used to estimate the propagation delay and transition time of a CMOS inverter driving a resistive-capacitive interconnect line. Since the shape of the output waveform is now known, (7) and (8) can also be used with (6) to estimate the short-circuit power dissipation of a CMOS gate loading the high impedance interconnect line, as is described in Section III.

The maximum error for the transition time for RC loads ranging from 10 Ω to 1000 Ω and 10 fF to 1 pF and for two different short channel CMOS technologies (0.8 μm and 1.2 μm CMOS) is 27%. The maximum error for the propagation delay is 25% over the same ranges and technologies. As the capacitance increases to 1 pF, the error of the propagation delay generally decreases to less than 20%. A similar decrease occurs for the transition time. Furthermore, both errors generally decrease with increasing load resistance.

The improved accuracy with increasing load resistance and capacitance is due to the RC load dominating the device parasitics, specifically, the source and drain capacitance, thereby improving the accuracy of the transistor I-V model for large RC loads. These device parasitic impedances are not included in the I-V model described in (2) but are considered by SPICE. This behavior also explains why the accuracy improves as the geometric size of the transistors becomes smaller, making the parasitic device resistances and capacitances smaller. Thus, these expressions for the propagation delay and transition time of a CMOS inverter driving an RC load become more accurate for

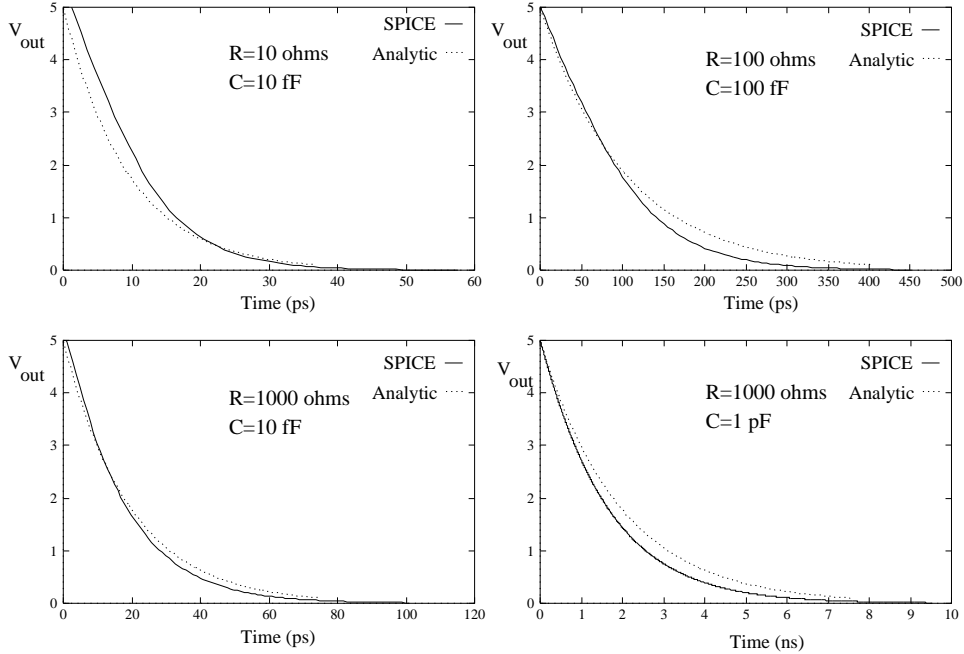


Fig. 3. Output response of a CMOS inverter driving an RC load.

Table I. Propagation delay t_{PD} and transition time t_t of an inverter driving an RC load (0.8 μm CMOS technology).

Load Resistance	Load Capacitance	t_t		t_{PD}		% Error	
		Analytic	SPICE	Analytic	SPICE	t_t	t_{PD}
10 Ω	.01 pF	21 ps	22 ps	6.5 ps	8.7 ps	4%	25%
10 Ω	.1 pF	215 ps	176 ps	65 ps	70 ps	22%	7%
10 Ω	1 pF	2.2 ns	1.7 ns	649 ps	680 ps	27%	4%
100 Ω	.01 pF	24 ps	22 ps	7.2 ps	8.8 ps	6%	19%
100 Ω	.1 pF	235 ps	187 ps	71 ps	73 ps	25%	2%
100 Ω	1 pF	2.4 ns	1.9 ns	712 ps	711 ps	25%	0%
1000 Ω	.01 pF	44 ps	39 ps	13 ps	13 ps	13%	0%
1000 Ω	.1 pF	444 ps	365 ps	133 ps	115 ps	22%	16%
1000 Ω	1 pF	4.4 ns	3.6 ns	1.3 ns	1.1 ns	22%	18%

higher RC loads and more aggressive submicrometer technologies, the regime of greatest interest.

III. Power Estimation

Power consumption has become one of the premier issues in VLSI circuit design. There are two primary contributions to the total transient power dissipated by a CMOS inverter, dynamic power dissipation and short-circuit power dissipation [8–11, 16, 17]. The short-circuit power is often neglected since the dynamic

power is assumed to be dominant. As described below and in [8–11, 16, 17], the magnitude of the short-circuit power is load dependent, and it is shown in this paper that short-circuit power can be a significant portion of the total transient power dissipation.

Dynamic power is briefly discussed in subsection A. In subsection B, an analysis of short-circuit power is presented, and a closed-form model is proposed. In subsection C, the power dissipated by the lossy resistive element of the RC load is discussed and modeled. Finally, some concluding remarks pertaining specifi-

cally to estimating the power of an RC loaded CMOS inverter are offered in subsection D.

A. Dynamic Power

Dynamic power is due to the energy required to charge and discharge a load capacitance C and is characterized by the familiar equation, CV^2f , where V is the source voltage and f is the switching frequency. The dynamic power is independent of the load resistance. For example, the dynamic power dissipation of a single CMOS inverter driving an RC load ranges from 35 μW to 125 μW for capacitive loads ranging from 0.3 pF to 1 pF and assuming a 5 volt power supply with the inverter switching every 10 MHz.

B. Short-Circuit Power

In subsection B.1, an expression for modeling the short-circuit power in a CMOS inverter is presented. This expression is analyzed and compared to SPICE in subsection B.2. In subsection B.3, a comparison of the short-circuit power to the total transient power dissipation as a function of load resistance is presented.

B.1. Analytic Expression of Short-Circuit Power. The logic stage following a large RC load may dissipate significant amounts of short-circuit power due to the degraded waveform originating from the CMOS inverter driving an RC load (see Figure 4). During the region where the input signal is transitioning between V_{TN} and $V_{DD} + V_{TP}$, a DC current path exists between V_{DD} and ground. The excess current dissipated during this region is called the short-circuit (or crossover) current [16]. Short-circuit current occurs due to a slow input transition, and for a balanced inverter, the peak current occurs near the middle of the input transition. An example of short-circuit current is shown by the solid line in the lower graph of Figure 5, *i.e.*, the SPICE-derived data.

The total short-circuit current I_{SC} can be estimated by modeling I_{SC} as a triangle. Therefore, the integral of I_{SC} is the area of a triangle, $\frac{1}{2} \text{base} \times \text{height}$. In terms of the short-circuit current, the height can be modeled as I_{peak} and the base can be modeled as t_{base} (see Figure 5). I_{peak} is the maximum saturation current of the load transistor and depends on both V_{GS} and V_{DS} , therefore I_{peak} is both input waveform and load dependent. t_{base}

is the time during which both the P-channel and the N-channel transistors are turned on, permitting a DC current path to exist between V_{DD} and ground. This time occurs over the region, $V_{TN} \leq V_{in} \leq V_{DD} + V_{TP}$. Therefore, t_{base} is found from the difference between (7) and (8), $|(t_{V_{TP}} - t_{V_{TN}})|$. The area defined by this triangle is $\frac{1}{2} I_{peak} \times t_{base}$, which models the total short-circuit current I_{SC} sourced by a CMOS inverter due to a non-step input [11].

The total short-circuit current multiplied by f and V_{DD} is the short-circuit power. The short-circuit power dissipation P_{SC} of the following stage for one transition (either rising or falling edge) can therefore be approximated by

$$P_{SC} = \frac{1}{2} I_{peak} t_{base} V_{DD} f. \quad (9)$$

Subtracting (7) from (8) forms the logarithmic quotient, $t_{base} = |\ln(\frac{V_{TN}}{V_{DD} + V_{TP}})| \frac{C + \mathcal{U}_{do} RC}{\mathcal{U}_{do}}$. By inserting this expression for t_{base} into (9), the short-circuit power dissipation P_{SC} of a CMOS inverter following a lumped RC load over both the rising and falling transitions is

$$P_{SC} = \left| \ln \left(\frac{V_{TN}}{V_{DD} + V_{TP}} \right) \right| \frac{C + \mathcal{U}_{do} RC}{\mathcal{U}_{do}} I_{peak} f V_{DD}. \quad (10)$$

B.2. Analysis of the Short-Circuit Power Dissipation Expression. The short-circuit power derived from (10) for a wide variety of RC loads between the CMOS inverter stages shown in Figure 4 is compared with SPICE in Table II. The RC load of the driving inverter is described in the first two columns of Table II. The short-circuit power predicted by (10) and derived from SPICE is shown in the third and fourth columns, respectively. The per cent error between the analytical expression and SPICE is shown in the final column.

For smaller RC loads, hence, faster transition times, there is negligible short-circuit power since a direct path from the power supply to ground does not exist for any significant time. The short-circuit power becomes non-negligible when larger interconnect loads between the two CMOS stages cause a transition time of significant magnitude (*e.g.*, a t_t greater than 0.5 ns for a 0.8 μm CMOS inverter). At this borderline value, the analytical P_{SC} differs from SPICE by a maximum of 41%. As the RC load and transition time increase, the analytical model more closely predicts the short-circuit current derived from SPICE. For RC loads exceeding 0.1 ns, errors less than 15% are attained. Fur-

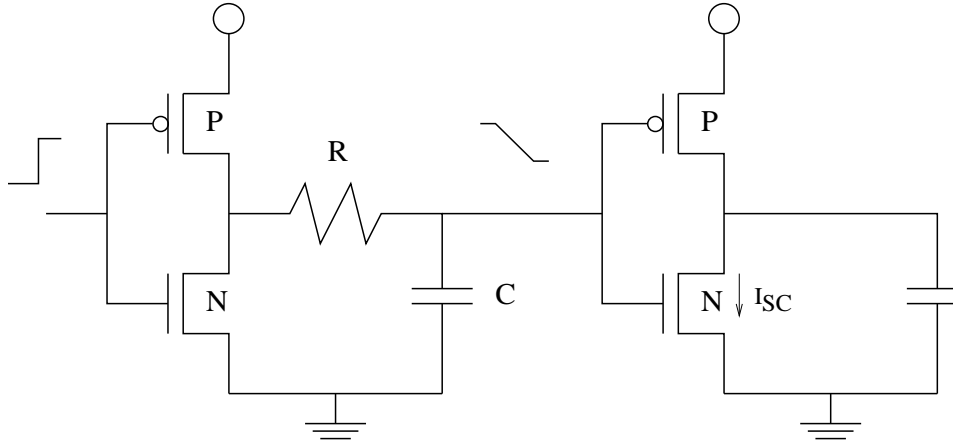


Fig. 4. Non-step input driving CMOS inverter stage creates short-circuit power.

Table II. Estimate of short-circuit power dissipated by a CMOS inverter (0.8 μm CMOS technology).

Load Resistance	Load Capacitance	Power (μW)		
		$f = 10 \text{ MHz}, V_{DD} = 5.0 \text{ V}$		
		Analytic	SPICE	% Error
10 Ω	.3 pF	1.4	.99	41%
10 Ω	.5 pF	3.9	3.22	21%
10 Ω	1 pF	12.4	11.1	12%
100 Ω	.3 pF	1.71	1.23	39%
100 Ω	.5 pF	4.68	3.83	22%
100 Ω	1 pF	13.8	12.7	9%
1000 Ω	.3 pF	5.85	5.2	12%
1000 Ω	.5 pF	13.0	12.2	7%
1000 Ω	1 pF	34.2	33.8	1%

thermore, the short-circuit power becomes a significant portion of the total power dissipation when the CMOS inverter is loaded by larger RC loads, creating long transition times. It is this condition that is of greatest interest when considering short-circuit power in resistively loaded CMOS inverters.

The error of the analytical expression for P_{SC} can be bounded by the RC time constant describing the interconnect load impedance. For a 0.8 μm CMOS technology, the per cent error is less than 15% for an RC time constant more than 0.1 ns. For an RC time constant less than 0.1 ns, the per cent error increases to approximately 40%.

One source of error in estimating the short-circuit power derived from (9) can be found by examining the transition time. The analytical solution to the transi-

tion time, (6), generally yields pessimistic results when compared to SPICE (see Table II). By inserting these pessimistic transition times into (9), the resulting short-circuit power is also pessimistic, as demonstrated in Table II.

Another source of error is caused by signal overshoot of fast transient waveforms. This parasitic-induced overshoot may increase V_{DS} above V_{DD} or below ground. This overshoot occurs early during the transition time and causes current to flow opposite to the expected direction, thereby reducing the total short-circuit current. This behavior, in turn, reduces the total short-circuit power, increasing the discrepancy between SPICE and (10), which does not consider transient overshoot. The phenomenon of signal overshoot can be seen in Figure 5.

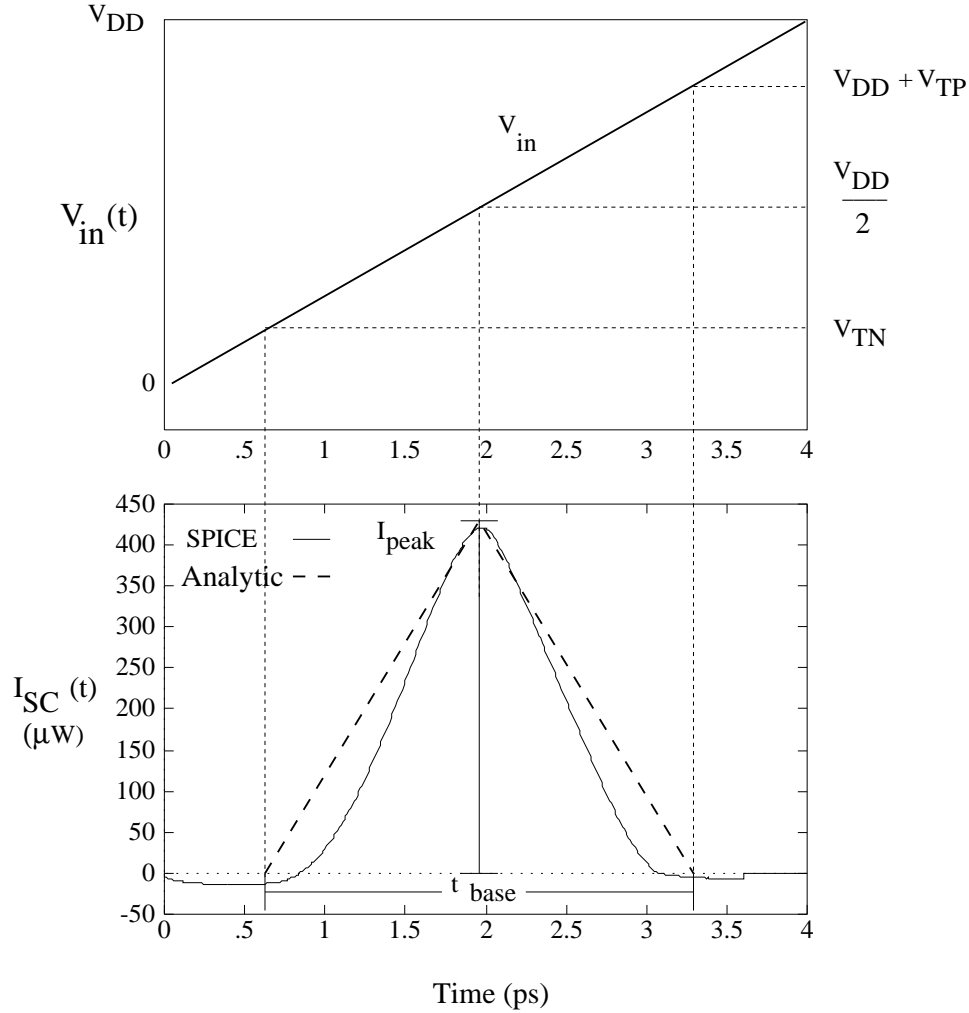


Fig. 5. Graphical estimation of short-circuit current dissipation (0.8 μm CMOS technology).

B.3. Short-Circuit Power as Compared to the Total Transient Power. For a given supply voltage and frequency, dynamic power dissipation depends only on the load capacitance and does not depend on the input waveform shape or load resistance. In contrast, the short-circuit power dissipation changes with both input waveform shape and output load resistance and capacitance. The ratio of the short-circuit power to the total transient power (the sum of the dynamic and short-circuit power) of a CMOS inverter with respect to the load resistance R for a given load capacitance C is shown in Figure 6. Note that with increasing load resistance, the short-circuit power dissipation cannot be neglected, since, as shown in Figure 6, it can comprise more than 20% of the total transient power dissipation.

C. Resistive Power Dissipation

In resistive interconnect, power is not only dissipated when charging and discharging the load capacitance, but power is also dissipated by the load resistance. This power dissipation can be quantified by $\int i^2 R$, where i is the current through the load resistance. The identical current that is discharged by the capacitor flows through the resistor. This capacitive current is $I_C = C \frac{dV_{out}}{dt}$. Therefore, by taking the derivative of (4), the instantaneous current through a resistive load $i_R(t)$ is given by

$$i_R(t) = \frac{-\mathcal{U}_{do}}{1 + \mathcal{U}_{do}R} V_{out}(0) e^{\frac{-\mathcal{U}_{do}}{\mathcal{U}_{do}RC+C}t}, \quad (11)$$

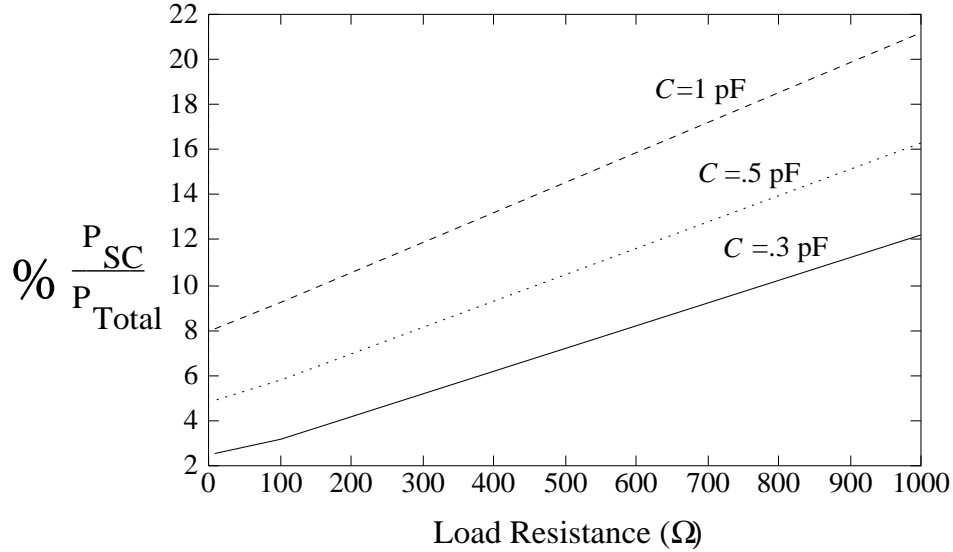


Fig. 6. Ratio of short-circuit power to total transient power versus load resistance for varying load capacitance.

and the average resistive power dissipation is given by

$$P_R = f \int_0^t \left(\frac{-\bar{U}_{do}}{1 + \bar{U}_{do}R} V_{out}(0) e^{\frac{-\bar{U}_{do}}{\bar{U}_{do}RC+C}t} \right)^2 R dt. \quad (12)$$

After integration, (12) becomes

$$P_R = \frac{f RC \bar{U}_{do} V_{out}^2(0)}{2(1 + \bar{U}_{do}R)} \left(1 - e^{\frac{-\bar{U}_{do}}{\bar{U}_{do}RC+C}2t} \right). \quad (13)$$

The resistive power dissipated for different RC loads calculated from (13) is shown in Table III. The load resistance R and capacitance C are listed in the first two columns, respectively. The power dissipated by the interconnect resistance determined from (13) and from SPICE are shown in the third and fourth columns, respectively. The per cent error of the analytic expression as compared to SPICE is shown in the final column. Note that the per cent error is less than 15% and typically less than 6%.

D. Summary

An expression for estimating the dynamic, short-circuit, and resistive power in CMOS inverter chains has been presented. For RC loads greater than .1 ns (assuming a 0.8 μm CMOS technology), the expression for the short-circuit power is accurate to within 15% of SPICE. These larger RC loads are of interest because short-circuit power can account for more than

20% of the total transient power dissipation. Furthermore, another source of power dissipation is introduced by the resistance of long interconnect. An expression for resistive power dissipation is also presented in this section. This expression has an error of less than 15% as compared to SPICE.

When considering power in interconnect, the resistive component cannot be neglected. The resistance of long interconnects not only contributes directly to the power dissipated due to the resistive component, but also causes longer transition times, leading to greater short-circuit power dissipation. Both short-circuit and resistive power dissipation along with dynamic power have been modeled with good accuracy.

IV. Conclusions

A simple yet accurate expression for the output voltage of a CMOS inverter as a function of time driving a resistive-capacitive load is presented. With this expression, equations characterizing the propagation delay and transition time of a CMOS inverter driving an RC load are presented. These expressions are accurate to within 25% of SPICE for a wide variety of RC loads. Furthermore, since the output waveform of this circuit is accurately modeled, the short-circuit power dissipation of the following CMOS stage loading the interconnect line can be accurately estimated to within 15% for highly resistive loads. The resistive power dissipation can be modeled to within 15% error for RC

Table III. The resistive power dissipated by a CMOS inverter driving an RC load (0.8 μm CMOS technology).

Load Resistance	Load Capacitance	Power (μW) $f = 10 \text{ MHz}, V_{DD} = 5.0 \text{ V}$		
		Analytic	SPICE	Error
10 Ω	.01 pF	.0137	.0135	1%
10 Ω	.1 pF	.137	.139	1%
10 Ω	1 pF	1.37	1.39	1%
100 Ω	.01 pF	.125	.118	6%
100 Ω	.1 pF	1.25	1.29	3%
100 Ω	1 pF	12.5	13.1	5%
1000 Ω	.01 pF	.658	.703	6%
1000 Ω	.1 pF	6.58	7.61	13%
1000 Ω	1 pF	65.8	76.8	14%

loads ranging from 0.1 ps to 1 ns. Therefore, due to the simplicity and accuracy of these expressions, the delay and power characteristics of a CMOS inverter driving a high impedance RC interconnect line can be efficiently estimated.

Appendix—Determining I_{do} and V_{do}

The alpha-power law model parameters, I_{do} and V_{do} , describe the maximum drain current and drain saturation voltage, respectively, where $V_{GS} = V_{DD}$ [10]. For increased accuracy of the delay expressions shown in section IIB, I_{do} and V_{do} may need to be adjusted for a specific CMOS technology. Initially, these two parameters of the alpha-power law model are determined as explained by Sakurai in [10]. With these parameters, an initial estimate of the propagation delay and transition time for any RC load for a specific CMOS technology can be made using (5) and (6), respectively.

These analytical estimates are compared to SPICE for a variety of RC load impedances. In order to improve the accuracy of the analytical expressions, I_{do} and V_{do} can be curve fit to SPICE. This process is performed only once for a given technology.

The adjustment of I_{do} is performed by determining

$$k_{PD} = \frac{C}{\bar{U}_{do} \left(\frac{t_{PDS}}{.693} - RC \right)} \quad (14)$$

and

$$k_{tt} = \frac{C}{\bar{U}_{do} \left(\frac{t_S}{2.2} - RC \right)}, \quad (15)$$

where t_{PDS} and t_S are the SPICE-derived propagation delay and transition times for the range of RC loads, i.e., $C = 10 \text{ fF}, 100 \text{ fF}, 1 \text{ pF}$ and $R = 10, 100, 1000 \Omega$. The factors k_{PD} and k_{tt} across this range of loads are averaged, and the result is k_{avg} ,

$$k_{avg} = \frac{1}{2} \sum_{i=1}^n \frac{k_{PD}}{n} + \frac{1}{2} \sum_{i=1}^n \frac{k_{tt}}{n}. \quad (16)$$

V_{do} is divided by k_{avg} or I_{do} is multiplied by k_{avg} . These analytical delay expressions produce results that yield values for the propagation delay and transition time that are the least square error from SPICE for this specific CMOS technology.

Acknowledgments

This research was supported in part by the National Science Foundation under Grant No. MIP-9208165 and Grant No. MIP-9423886, the Army Research Office under Grant No. DAAH04-93-G0323, and by a grant from the Xerox Corporation.

References

1. S. Bothra, B. Rogers, M. Kellam, and C. M. Osburn, "Analysis of the effects of scaling on interconnect delay in ULSI circuits," *IEEE Transactions on Electron Devices* ED-40(3), pp. 591–597, March 1993.
2. H. B. Bakoglu and J. D. Meindl, "Optimal Interconnection Circuits for VLSI," *IEEE Transactions on Electron Devices* ED-32(5), pp. 903–909, May 1985.
3. S. Dhar and M. A. Franklin, "Optimum Buffer Circuits for Driving Long Uniform Lines," *IEEE Journal of Solid-State Circuits* SC-26(1), pp. 32–40, January 1991.

4. M. Nekili and Y. Savaria, "Optimal Methods of Driving Interconnections in VLSI Circuits," *Proceedings of the IEEE International Symposium on Circuits and Systems*, pp. 21–23, May 1992.
5. C. Y. Wu and M. Shiau, "Delay Models and Speed Improvement Techniques for RC Tree Interconnections Among Small-Geometry CMOS Inverters," *IEEE Journal of Solid-State Circuits* SC-25(5), pp. 1247–1256, October 1990.
6. J. Cong and C.-K. Koh, "Simultaneous Driver and Wire Sizing for Performance and Power Optimization," *IEEE Transactions on VLSI Systems* VLSI-2(4), pp. 408–425, December 1994.
7. R. J. Antinone and G. W. Brown, "The Modeling of Resistive Interconnects for Integrated Circuits," *IEEE Journal of Solid-State Circuits* SC-18(2), pp. 200–203, April 1983.
8. L. Bisdounis, S. Nikolaidis, O. Koufopavlou, and C. E. Goutis, "Modeling the CMOS Short-Circuit Power Dissipation," *Proceedings of the IEEE International Symposium on Circuits and Systems*, pp. 4.469, 4.472, May 1996.
9. A. M. Hill and S.-M. Kang, "Statistical Estimation of Short-Circuit Power in VLSI Circuits," *Proceedings of the IEEE International Symposium on Circuits and Systems*, pp. 4.105–4.108, May 1996.
10. A. Hirata, H. Onodera, and K. Tamaru, "Estimation of Short-Circuit Power Dissipation and Its Influence on Propagation Delay for Static CMOS Gates," *Proceedings of the IEEE International Symposium on Circuits and Systems*, pp. 4.751–4.754, May 1996.
11. V. Adler and E. G. Friedman, "Delay and Power Expressions for a CMOS Inverter Driving a Resistive-Capacitive Load," *Proceedings of the IEEE International Symposium on Circuits and Systems*, pp. 4.101–4.104, May 1996.
12. A. I. Kayssi, K. A. Sakallah, and T. M. Burks, "Analytical Transient Response of CMOS Inverters," *IEEE Transactions on Circuits and Systems I: Fundamental Theory and Applications* CAS I-39(1), pp. 42–45, January 1992.
13. N. Hedenstierna and K. O. Jeppson, "CMOS Circuit Speed and Buffer Optimization," *IEEE Transactions on Computer-Aided Design* CAD-6(2), pp. 270–281, March 1987.
14. T. Sakurai and A. R. Newton, "Alpha-Power Law MOSFET Model and its Applications to CMOS Inverter Delay and Other Formulas," *IEEE Journal of Solid-State Circuits* SC-25(2), pp. 584–594, April 1990.
15. H. Shichman and D. A. Hodges, "Modeling and Simulation of Insulated-Gate Field-Effect Transistor Switching Circuits," *IEEE Journal of Solid-State Circuits* SC-3(3), pp. 285–289, September 1968.
16. H. J. M. Veendrick, "Short-Circuit Dissipation of Static CMOS Circuitry and Its Impact on the Design of Buffer Circuits," *IEEE Journal of Solid-State Circuits* SC-19(4), pp. 468–473, August 1984.
17. S. R. Vemuru and N. Scheinberg, "Short-Circuit Power Dissipation Estimation for CMOS Logic Gates," *IEEE Transactions on Circuits and Systems I: Fundamental Theory and Applications* CAS I-41(11), pp. 762–766, November 1994.

Victor Adler received the B.S. degree in electrical engineering and the B.A. degree in Computer Science from Duke University, Durham, North Carolina in 1992. He received the M.S. degree in electrical engineering from the University of Rochester, Rochester, NY in 1993 and is currently working toward his Ph.D. degree in electrical engineering at the University of Rochester.

He was an IBM Watson Scholar and worked preprofessionally at IBM Microelectronics, Burlington, Vermont between 1988 and 1992 in the areas of final module test, packaging, circuit macro development, and standard cell design. He has been a Teaching and Research Assistant at the University of Rochester since 1993. His research interests include design techniques for high performance CMOS and superconductive technologies.

Eby G. Friedman was born in Jersey City, New Jersey in 1957. He received the B.S. degree from Lafayette College, Easton, PA in 1979, and the M.S. and Ph.D. degrees from the University of California, Irvine, in 1981 and 1989, respectively, all in electrical engineering.

He was with Philips Gloeilampen Fabrieken, Eindhoven, The Netherlands, in 1978 where he worked on the design of bipolar differential amplifiers. From 1979 to 1991, he was with Hughes Aircraft Company, rising to the position of manager of the Signal Processing Design and Test Department, responsible for the design and test of high performance digital and analog IC's. He has been with the Department of Electrical Engi-

neering at the University of Rochester, Rochester, NY, since 1991, where he is an Associate Professor and Director of the High Performance VLSI/Design and Analysis Laboratory. His current research and teaching interests are in high performance microelectronic design and analysis with application to high speed portable processors and low power wireless communications.

He has authored two book chapters and many papers in the fields of high speed and low power CMOS design techniques, pipelining and retiming, and the theory and applications of synchronous clock distribution networks, and has edited one book, *Clock Distribution Networks in VLSI Circuits and Systems* (IEEE Press, 1995). Dr. Friedman is a Senior Member of the

IEEE, a Member of the editorial board of *Analog Integrated Circuits and Signal Processing*, Chair of the VLSI Systems and Applications CAS Technical Committee, Chair of the VLSI track for ISCAS '96 and '97, and a Member of the technical program committee of a number of conferences. He was a Member of the editorial board of the *IEEE Transactions on Circuits and Systems II: Analog and Digital Signal Processing*, Chair of the Electron Devices Chapter of the IEEE Rochester Section, and a recipient of the Howard Hughes Masters and Doctoral Fellowships, an NSF Research Initiation Award, an Outstanding IEEE Chapter Chairman Award, and a University of Rochester College of Engineering Teaching Excellence Award.